Nano Energy (2014) 7, 161–169

Available online at www.sciencedirect.com

ScienceDirect

journal homepage: www.elsevier.com/locate/nanoenergy

RAPID COMMUNICATION

Resilient aligned carbon nanotube/graphene sandwiches for robust mechanical energy storage

Cheng Tang, Qiang Zhang*, Meng-Qiang Zhao, Gui-Li Tian, Fei Wei

Beijing Key Laboratory of Green Chemical Reaction Engineering and Technology, Department of Chemical Engineering, Tsinghua University, Beijing 100084, PR China

Received 9 March 2014; received in revised form 24 April 2014; accepted 12 May 2014
Available online 20 May 2014

KEYWORDS
Energy storage;
Hybrid;
Carbon nanotube;
Graphene;
Hierarchical nanostructures

Abstract
The use of microscale flexible mechanical energy storage devices, instead of traditional electrochemical energy storage devices based on supercapacitors and Li-ion batteries, is highly considered for portable electronics, actuators, and meso-micro scale systems. The selection of resilient and robust building blocks is the first step for high energy-density mechanical energy storage system. Herein, alternative aligned carbon nanotubes (CNTs) and graphene were effectively sandwiched into freestanding sp^2 all-carbon hybrids, rendering the excellent loading transfer in the three-dimensional framework. The millimeter-scale aligned CNT/graphene sandwiches could be repeatedly compressed at high strains ($\varepsilon > 90\%$), with a highest energy absorption density of 237.1 kJ kg^{-1}, an ultrahigh power density of 10.4 kW kg^{-1}, and a remarkable efficiency of 83% during steady operation, providing novel nanocomposites with outstanding mechanical energy storage performance comparable to electrochemical batteries and bridging nanoscopic structures to micro- and mesoscale applications.

1. Introduction

The broad applications of portable electronics and electric vehicles worldwide stimulate the development of energy storage devices or physical media toward higher power density and energy density. Among various strategies, mechanical energy storage that is carried out by conversion into kinetic energy *via* rotating, or potential energy *via* stretching, compression, or elevation has been widely applied nowadays [1]. In fact, the original utilization of mechanical energy storage, the bow, even predates recorded history. While the string of a bow is drawn back, compressive force is exerted on the elastic limbs. The limbs are flexed with higher potential energy, which can be transformed into kinetic energy of the arrow after releasing the string. Consequently, mechanical properties of the

*Corresponding author.
E-mail address: zhang-qiang@mails.tsinghua.edu.cn (Q. Zhang).

http://dx.doi.org/10.1016/j.nanoen.2014.05.005
2211-2855/

materials for limbs are of significant importance to the performance of the bow. The combination of materials that are more resilient in compression or tension, such as horn, sinew, fiberglass, and carbon fibers, always brings more powerful bows with better mechanical energy storage and release performances. The pumped hydropower storage system based on mechanical energy storage can also date back to ancient times, and it has still been widely developed and employed in the modern society. Other mechanical energy storage systems, such as flywheels storing mechanical energies by the use of a rapidly rotating flywheel [2], compressed air storing mechanical energies in a confined underground cave or abandoned mine [1], and steel springs storing mechanical energies by their elasticity, were also widely employed. However, the above mentioned mechanical energy storage systems were based on traditional fluid or elastic solids, which offer limited energy density and always operate at a bulk scale. With the increasing requirements on portable electronics, actuators, meso-micro scale systems, the use of microscale flexible mechanical energy storage devices, instead of traditional electrochemical energy storage devices based on supercapacitors and Li-ion batteries, is highly required. Recently, there are breakthroughs on harnessing the fluctuating and transient by "nanogenerators" to realize conversion between mechanical energy and electrical energy using piezoelectric nanogenerator [3,4], triboelectric nanogenerator [5], electromechanical bimorph actuator [6] and free surfaces [7] with unique actuation characteristics and exceedingly high efficiency.

Just like the construction of a stronger bow, the selection of resilient and robust building blocks is the first step for high energy-density mechanical energy storage system. The intrinsic mechanical properties determine their potentials for robust devices with ultra-high energy density and good recovery rate. Both carbon nanotubes (CNTs) and graphene possess exceptional mechanical properties with high tensile strength of 63 and 125 GPa as well as Young modulus of 1.25 [8] and 1.0 TPa [9], respectively. CNT films behave as open-cell foams with nanotubes as elastic struts [10]. The energy storage density of CNT bundles under tensile loading is calculated to be at least three orders larger than that of steel springs, and even under practical considerations, it is still comparable to batteries [11,12]. In theoretical calculations, CNT ropes are also demonstrated to store mechanical energy *via* twisting, stretching, bending and compressing reversibly with a capacity 4 to 10 times higher than that of Li-ion batteries [13]. The individual CNTs have a mechanical energy density as high as 4050 kJ kg^{-1} [14]. The rational combination of CNT sponge with array constructs highly compressible and elastic macroscopic structures with extended energy absorption range and high energy dissipation [15-18]. However, the potential applications in mechanical energy storage for CNTs have greatly suffered from the difficulty of device assembly due to the nano-sized structure.

Fine combination of one-dimensional (1D) and two-dimensional (2D) building blocks which leads to the formation of hierarchical three-dimensional (3D) composites can usually inherit full advantages of the component materials, or even bring about unexpected properties for unique applications [19-21]. For instance, stable sponge-like structure made of 1D CNTs allows excellent compressibility tunable up to 90% volume shrinkage, and the ability to recover most of volume by free expansion [22]. Graphene has been employed to fabricate multichannel and repeatable self-healing polymeric materials with enhanced mechanical properties and excellent healing efficiency higher than 98%. [23] Chemically converted graphene aerogels with density as low as 3.0 mg cm^{-3} show excellent resilience and can completely recover after more than 90% compression, which are promising as compliant and energy-absorbing materials [24]. The alternate combination of vertically aligned CNTs and 2D inorganic sheets made the resultant 3D hybrid architecture more ductile and resilient [25], and the mechanical energy absorption performances were enhanced greatly in contrast to CNT aggregates [25,26]. 3D CNT/graphene hybrids with extraordinary capacitive performance and storage density were available by facile incorporation of CNTs and graphene through *in situ* growth [27-31]. When the CNTs graft on graphene, they serve as spacers to inhibit the stacking of graphene flakes; meanwhile, the graphene interlinked with CNTs hinders the strong entanglement of tubes [32]. The fine arrangement of 1D CNTs and 2D graphene is highly expected to obtain hybrid sp^2 carbon with ordered structures as well as unique mechanical properties [33], although the current chemical routes *via* self assemble, selective oxidation, electrodeposition, and *in situ* growth [34-39] offer very poor ability to vertically aligned and high-density CNTs on graphene without barriers. It is highly expected to integrate CNTs with graphene into 3D ordered, alternative, highly compressible macroscopic structures instead of entangling or stacking into randomly distributed agglomerates with the potential to full demonstration of the mechanical properties of CNT/graphene hybrids.

In this contribution, we explored the idea of *in situ* CVD of alternative aligned CNTs and graphene sheets to form freestanding 3D sp^2 carbon sandwiches for excellent mechanical energy storage. The reason we selected aligned CNTs rather than entangled CNTs is that aligned CNTs intrinsically exhibit excellent mechanical properties and super-compressible behavior [10,12]. The introduction of strong but flexible graphene sheets to the ends of aligned CNTs renders the resultant composites consisting of dense CNT arrays seamlessly linked by graphene sheets placed vertically to the *c*-axis of CNTs, guaranteeing the excellent stress transfer in the 3D framework. The aligned CNT/graphene sandwiches could be repeatedly compressed at high strains ($\varepsilon > 90\%$), with a highest energy absorption density of 237.1 kJ kg^{-1}, which is about 1700 times that of steel springs (0.14 kJ kg^{-1}) [40], a remarkable efficiency of 83% during steady operation, and an ultrahigh power density of 10.4 kW kg^{-1}. Such excellent mechanical energy storage performance is supposed to be available with particular-designed power supply systems, such as that with escapement mechanisms and piezoelectric cantilevers for CNT springs [12], thereby making this novel composite a new energy storage strategy comparable to electrochemical batteries and perhaps even approaching flywheels.

2. Results and discussion

Our strategy for the fabrication of aligned CNT/graphene sandwiches involves a two-step CVD growth method, which is

illustrated in Fig. 1. Typically, a layered material embedded with metal nanoparticles (NPs) in their interlayer spaces serves as the bifunctional catalysts for the growth of aligned CNT/graphene sandwiches (Fig. 1a). First, intercalated growth of aligned CNTs among the layered catalyst is carried out through a low-temperature CVD (L-T CVD) (Fig. 1b). Then, a high-temperature CVD (H-T CVD) was conducted subsequently to deposit graphene layers onto the surface of lamellar flakes of the layered catalyst (Fig. 1c). Sandwiched aligned CNT/graphene hybrids composed of alternating aligned CNTs and graphene materials were available by removal of the catalyst.

Herein, FeMo/vermiculite composed of exfoliated vermiculite (EV) with FeMo NPs supported on their interlayer surfaces was employed as the bifunctional catalysts for the two-step *in situ* growth of aligned CNT/graphene sandwiches. CVD of ethylene at a low-temperature of 650 °C was firstly carried out to achieve the intercalated growth of aligned CNTs on the metal catalysts. The growth of aligned CNTs also is beneficial to the metal NPs with stable size. The EV layers were pushed away from each other but their morphologies were well preserved, which provided diffusion pathway for the carbon source to reach the EV layer for uniform deposition of graphene layers on each EV layers at a high temperature of 950 °C. With the intercalation of aligned CNTs and graphene into EV, the flat sheets of vermiculites were obviously expended in length (Fig. 2a). The scanning electron microscopy (SEM) images shown in Fig. 2b and c reveal a periodical sandwich-like structure that aligned CNTs with a uniform length and good alignment were perpendicularly grown among the interlayer spaces of EV sheets.

Aligned CNT/graphene sandwiches with high carbon purity of 98.3 wt% are available after the removal of the FeMo/vermiculite catalysts by facile acid treatments (Fig. 2d–f). The as-obtained aligned CNT/graphene sandwiches exhibit the morphology of alternating aligned CNTs and continuous graphene sheets (Fig. 2e and f). There are nano-gaps between the two opposite aligned CNT/graphene structural units, which are resulted by the removal of the EV flakes (Fig. 2f). The transmission electron microscopy (TEM) images shown in Fig. 2g and h illustrate the morphology of the aligned CNT/graphene building blocks. The aligned CNTs were perpendicularly connected to the graphene sheet at the bottom, and two opposite structural units joined in the middle through the interlink of CNTs due to the opposite growth of two aligned CNT bundles (Fig. 2g). The aligned CNTs were multi-walled with a uniform length of 7–13 μm after 15 min CVD growth at 650 °C. The layer of graphene sheets was *ca.* 2–5 after 30 min deposition at 950 °C and was well tuned by varying the growth parameters (Fig. S1a). Strong 2D bands (~2670 cm^{-1}) were detected in the Raman spectra both for the graphene and aligned CNT/graphene sandwich samples, which was mainly contributed from the few-layered graphene (Fig. S1b). Five first-order Raman bands (G, D1, D2, D3, D4) at about 1580, 1350, 1620, 1500, 1200 cm^{-1} were taken into account for an unambiguous interpretation of the Raman spectra in the range of 1000-1800 cm^{-1} as shown in Fig. S1c–e. [41] The I_{D1}/I_G ratio for the aligned CNT/graphene sandwiches (1.48) was larger than that of aligned CNT array (1.16) or graphene (1.04) grown under the same conditions of the above-mentioned two-step CVD, respectively, which can be attributed to the inevitable defects at the junction areas between aligned CNTs and graphene sheets [32,42].

Regarding to the understanding of the aligned CNT/graphene sandwich architecture, the interface between the aligned CNTs and graphene is of paramount importance to their mechanical properties. Due to the non-uniform stress distribution of the network, the bond breakage, sheet fracture, and ripping off of the CNT arrays from graphene sheets were available [42]. Accordingly, a protensive and strong sonication method was used to tear a large amount of CNTs from the graphene layers to afford an unambiguous TEM image of the interface between the aligned CNT and graphene. After ultrasonic treatment for 120 min at a high power (300 W, 40 kHz), many CNTs were torn off, leaving a large amount of graphitic rings on the graphene sheets (Fig. 2i). The inset of Fig. 2i is a high resolution TEM image of a graphitic ring, showing the existence of a notch on the graphitic ring. Carbon nanorings are usually considered as super-short CNTs [43] or the graphene layers encapsulating outside of Fe nanoparticles. Herein, these nanorings represent the interface regions of CNTs and graphene for the

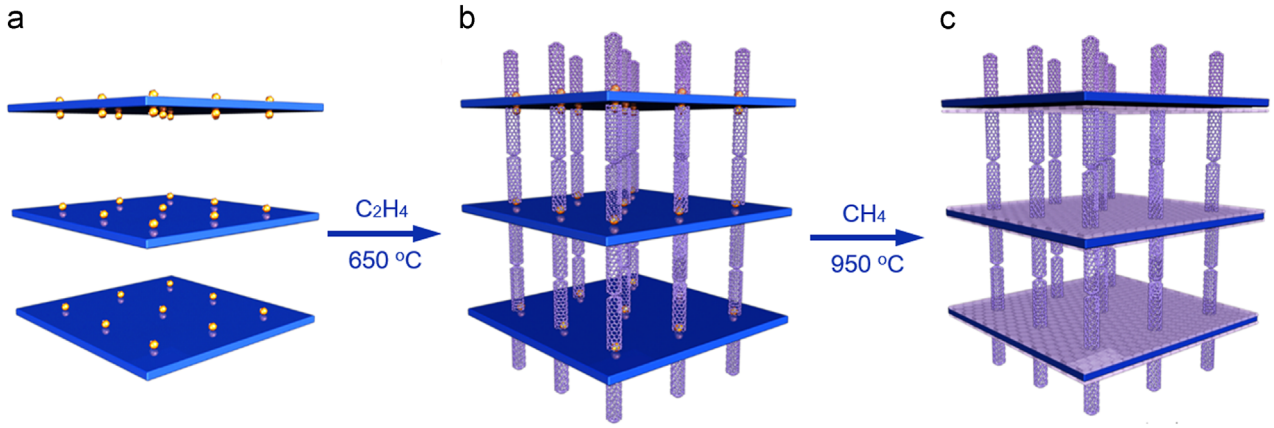

Fig. 1 Schematic illustration for the synthesis of aligned CNT/graphene sandwiches on bifunctional catalysts. (a) Metal NPs nucleated on the surface of EV flakes; (b) aligned CNTs opposite grown on EV flakes by a L-T CVD; (c) graphene sheets deposited on EV flake by H-T CVD for aligned CNT/graphene sandwich formation.

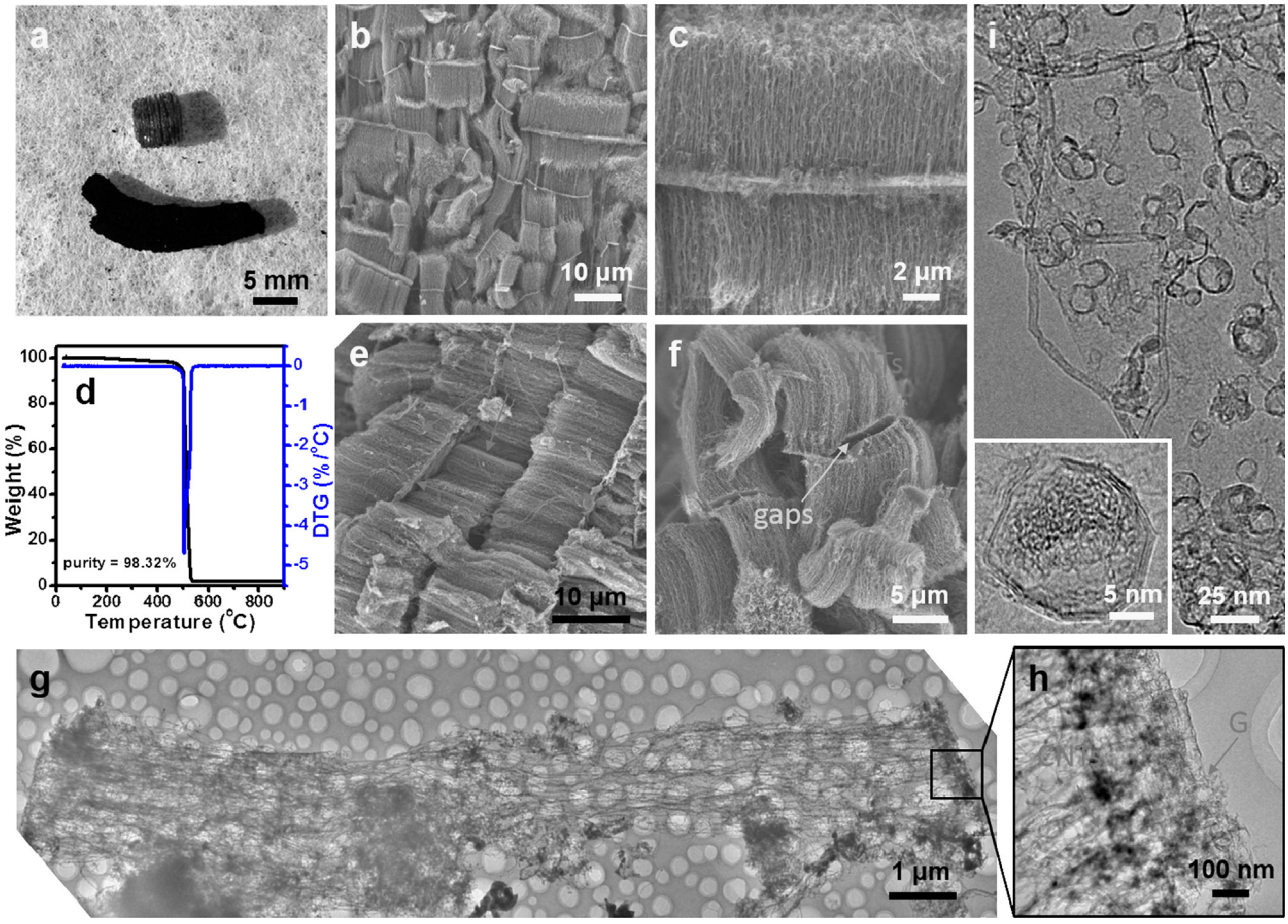

Fig. 2 Nanostructures of aligned CNT/graphene sandwiches. (a) Digital photograph of a block of EV catalyst (brown) and aligned CNT/graphene sandwich. ((b) and (c)) SEM images of aligned CNT/graphene/EV composite. (d) TGA curve of the aligned CNT/graphene sandwiches under O_2 atmosphere. ((e) and (f)) SEM images of the aligned CNT/graphene sandwiches. (f) showing continuous graphene sheets (yellow arrowed) at the bottom of aligned CNTs (red arrowed). The arrowed gaps were generated after the removal of the vermiculite flake. (g) TEM image of the aligned CNT/graphene sandwiches. (h) TEM image showing a typical view of the junction region of aligned CNTs and graphene. (i) TEM images of the sandwich sample prepared via protensive ultrasonic treatment. Multi-walled graphitic rings were observed, and the structure was further characterized by high-resolution TEM (inset), showing a notch (arrowed) on the ring.

as-fabricated aligned CNT/graphene sandwiches, which is probably resulted by the deposition of graphene layers around the roots of CNTs. This kind of structure is benefited to anchor CNTs on graphene and is important for the stress transfer between aligned CNTs and graphene sheets.

The unique features and unexpected properties of nanomaterials are always determined by their nanostructures. Herein, both the length of aligned CNTs and the lateral size of graphene sheets in the as-fabricated aligned CNT/graphene sandwiches were well tuned (Fig. S2). Fig. S2a-c clearly showed that the length of aligned CNTs increased from about 1 to 25 μm with the CNT growth time prolonged from 5 to 30 min. With the increase of the CNT length, the layer-to-layer distance of between the graphene sheets was expanded greatly. Meanwhile, the lateral size of the graphene sheets decreased a lot from the similar size of the EV flakes to about 1 μm due to the cracking of the EV flakes along with the intercalated growth of aligned CNTs (Fig. S2d-f). Larger free-standing aligned CNT/graphene sandwich blocks with a size from hundreds of micrometers to several centimeters can be fabricated depending on the lateral size of the EV particles (Fig. S2g and h).

Many reports have described the fabrication of CNT/graphene hybrids [27-32,34-37,44-48]. However, the as-obtained CNTs and graphene are always entangled with each other. The ordered 3D packing structures of aligned CNTs and graphene were hardly available. In other cases of the successful fabrication of aligned CNT/graphene hybrids, the aligned CNTs and graphene are always connected indirectly with a barrier layer [28,30,38,45,49,50]. Herein, the bifunctional FeMo/vermiculite catalyst is very effective to obtain high-quality aligned CNTs and graphene with a direct and intimate connection. The vermiculite is a kind of layered natural aluminosilicate that inherently contains various metal elements (*e.g.*, Fe, Mg, Al). After reduction under H_2 atmosphere, Fe NPs were formed on the pristine vermiculite sheets and promoted the CNT growth. Only entangle CNTs, however, were produced and the periodic pillar-layer structure was completely unavailable using the pristine EVs (Fig. S3). If the procedure was simplified to

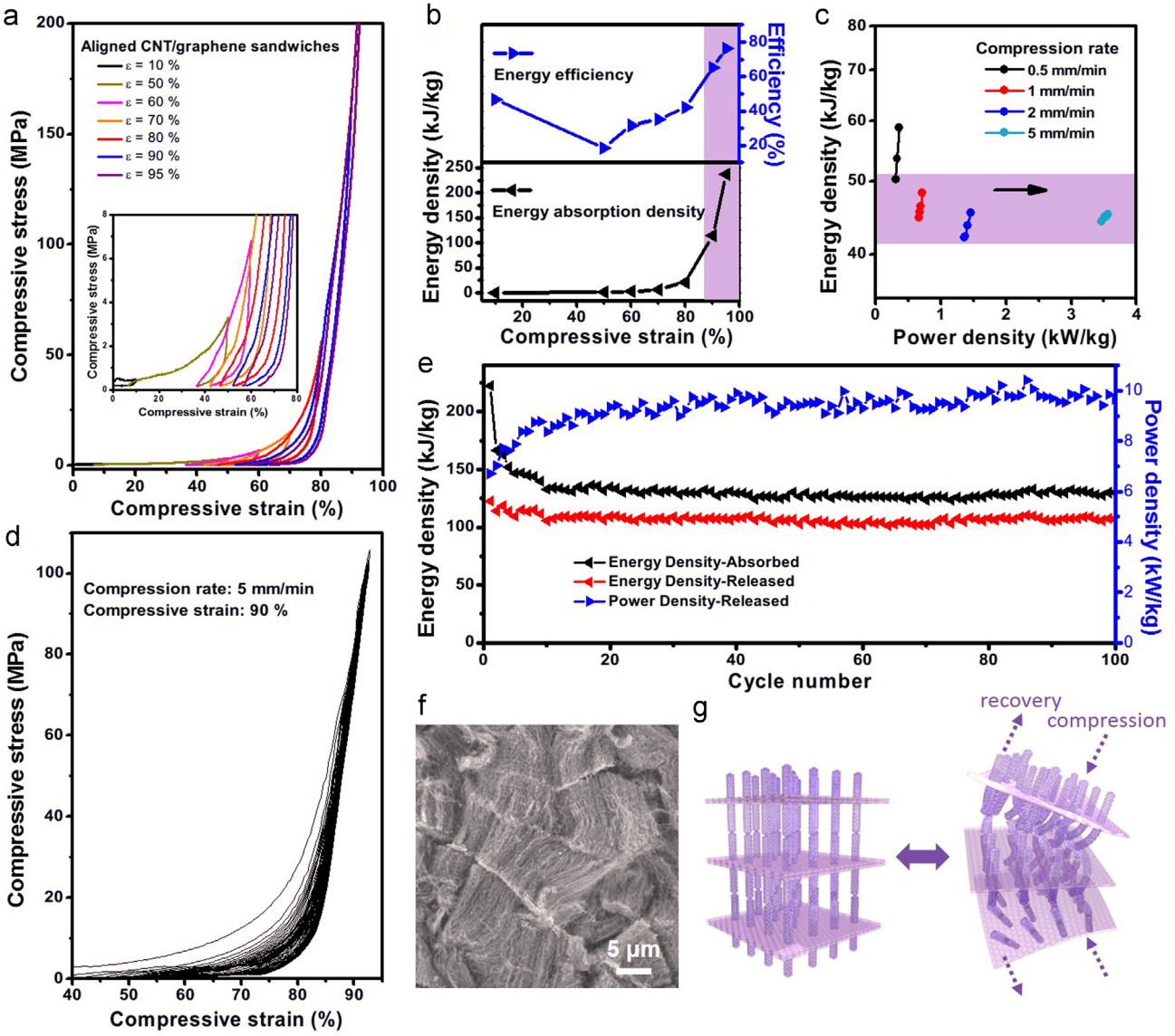

Fig. 3 Mechanical energy storage properties of the aligned CNT/graphene sandwiches. (a) Compressive stress-strain (σ-ε) curves of a freestanding block of aligned CNT/graphene sandwiches at a compression rate of 0.5 mm min^{-1}, and energy absorption density for each ε is shown in (b), indicating a higher density and efficiency of energy storage at higher strains. (c) Energy storage properties of the aligned CNT/graphene sandwiches at different compression rates. (d) Cyclic compressive σ-ε curves of a sandwich block at a set strain of 90% and a compression rate of 5 mm min^{-1}, and (e) shows the energy and power density of each cycle. The lengths of aligned CNTs in all the samples are *ca.* 10 μm. (f) SEM image of the sample after 100 cyclic compression, showing the maintenance of the sandwich-like structure. (g) Illustration of the compression and recovery performance of aligned CNT/graphene sandwiches.

one-step CVD growth of CNTs and graphene simultaneously, no successive graphene sheets were observed (Fig. S3e), in contrast to the as-obtained hybrids *via* two-step process (Fig. S3c and d). It was also demonstrated that reverse of the order of the two-step CVD was not applicable for the fabrication of aligned CNT/graphene sandwiches due to the fact that the deposition of graphene during the H-T CVD resulted in serious sintering of the metal NPs and thus hindered the subsequent growth of aligned CNTs. Therefore, the key issue for the fabrication of the novel aligned CNT/graphene architecture is that the high-quality aligned CNTs and graphene were separately grown on FeMo NPs and EV flakes at L- and H-T CVD, respectively.

The as-obtained aligned CNT/graphene sandwiches are of abundant porosity, excellent structural stability, and a hierarchical resilient structure, which render them as promising materials for mechanical energy storage. This bottom-up strategy that integrates CNTs and graphene into 3D networks enhances their intrinsic excellent properties and performance, and can even bridge the microscopic structure to meso- and macroscale applications.

The mechanical energy storage performance of the as-obtained aligned CNT/graphene sandwiches was evaluated through compression tests. A freestanding block of aligned CNT/graphene sandwiches with a size of 4 mm and a CNT length of *ca.* 10 μm was repeatedly tested at set strain

values ranging from 10 to 95% (Fig. 3a). The compressive stress-strain (σ-ε) curve illustrates two distinct regions, including initial plateau and subsequent densification region with different modulus. The gaps between structural units (Fig. 2f) of the sandwiches were firstly collapsed during the low-modulus region ($\sim$22.4 MPa), resulting in rapid deformation ($\varepsilon<70\%$) under low stress. With progressive increasing of the strain, the buckling and densification of aligned CNTs took place, making the stress increase rapidly. The compressive modulus approached as high as 2.3 GPa. The loading and unloading curves were distinct with a hysteresis loop, which represented the energy dissipation resulted from structure deformation during cyclic compressions (Fig. 3a and d) [12,14,25,51]. The nonlinear elasticity and hysteresis are two characteristic features of viscoelastic materials [52]. Energy absorbed or released during each compression was calculated by integrating the area under loading or unloading curves. Fig. 3b described the energy absorption density versus the strain, corresponding to the compression test of Fig. 3a. The energy absorption density increased rapidly from 0.27 kJ kg^{-1} ($\varepsilon=10\%$) to 237.1 kJ kg^{-1} ($\varepsilon=95\%$), while the dissipated energy was reduced from 53.4% to as low as 23.9%, indicating a higher density and efficiency of mechanical energy storage at higher strains. The maximum energy absorption density, 237.1 kJ kg^{-1}, was much higher than that of polymer foam (polystyrene, 10-37 kJ kg^{-1}) [26], powder (MgO nanoparticle, 15-45 kJ kg^{-1}) [26], agglomerated CNTs (15-70 kJ kg^{-1}) [26], graphene aerogel (0.76-1.26 kJ kg^{-1}) [24], CNT sponge (1.5-7.3 kJ kg^{-1}) [16,22], aligned CNTs-vermiculite composites (149 kJ kg^{-1}) [25], and about 1700 times that of steel springs (0.14 kJ kg^{-1}) [40].

For comparison, cyclic compressions of original EV particles, aligned CNTs obtained from the L-T CVD growth method using the FeMo/vermiculite catalyst, and aligned CNT/graphene sandwiches were conducted at a set strain of 50% (Fig. S4a). The original EV exhibited substantially the lowest energy absorption density of $\sim$0.64 kJ kg^{-1}, while a higher energy absorption density of $\sim$2.06 kJ kg^{-1} was achieved by the aligned CNTs. It was worthy to note that the aligned CNT/graphene sandwiches were with the highest energy absorption density of $\sim$4.68 kJ kg^{-1} ($\varepsilon=50\%$), which was more than two times of that of aligned CNTs derived from the same FeMo/vermiculite catalyst. This indicated that the integration of graphene materials to the end of aligned CNTs tended to make the composites stronger and more resilient with a higher compressive stress and energy density, and better recovery. SEM images of the samples after compression (Fig. S4b and c) showed that the ordered sandwich-like structure of aligned CNT/graphene sandwiches was well preserved after the high-strain compression, whereas, the ordered structure of aligned CNTs tended to be destroyed. This indicated that adjunction of layered graphene sheets vertically to the bottom of CNT arrays was a decisive factor for the maintenance of the freestanding sandwiched 3D network during high-strain compression, leading to their excellent mechanical resilient and energy storage performances.

The mechanical energy storage performance also depended on the loading rate. The energy density changed negligibly when the compression rate varied from 0.5 to 5 mm min^{-1} (Fig. 3c). However, the power density multiplied due to the shortened loading or retreating time. The optimized parameters were set for cyclic compression tests, in which the compression rate was set as 5 mm min^{-1} and the strain was set as 90%. The σ-ε curves revealed high energy absorption and excellent reversibility in a wide strain range of 50-90% (Fig. 3d). During the initial cycle, the absorbed energy density was very high, but it decreased in subsequent cycles. Such a phenomenon is known as 'preconditioning', which is commonly observed in soft-tissue materials [52]. After 10 cycles, the hysteresis loops reach a steady state, and the energy absorption density became stationary at around 130 kJ kg^{-1}, of which almost 83% is recoverable (Fig. 3e-g). The aligned CNT/graphene sandwiches maintained the alternating aligned CNT-graphene architecture even after 100 cyclic compressions (Fig. 3f), demonstrating that the 3D sandwiched nanocarbon structure rendered efficient stress transfer and excellent compression-resilience performance like springs (Fig. 3g). The as-obtained freestanding composite was all-carbon sandwich, which implied that the buckling or stretch of robust C-C bonds in the 3D architectures during cyclic compression and release render their astonishing performance as mechanical energy storage materials.

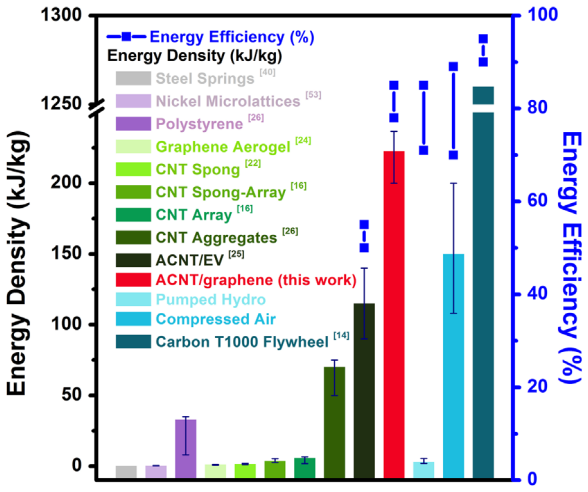

Fig. 4 Comparison of different mechanical energy storage materials and systems.

With a particularly well-designed power supply analogous to that for CNT springs [12], the impressive mechanical energy storage performances of aligned CNT/graphene sandwiches are potentially expected in practical applications. Among various mechanical energy storage materials, the aligned CNT/graphene sandwiches possess strong competitive edge in the energy density compared with different nanocarbon composites [16,22,24,26,53]; meanwhile, the energy density and efficiency are even comparable to some grid-scale mechanical energy storage systems, such as Pumped Hydro and Compressed Air Energy Storage, and even approaching flywheels (Fig. 4) [14]. Moreover, in contrast to other kinds of energy storage systems, such as electrochemical batteries and supercapacitors, the aligned CNT/graphene sandwiches exhibit competitive performance in energy storage devices, considering the comparative energy density and higher power density ($>$10 kW kg^{-1}).

3. Conclusions

A resilient aligned CNT/graphene sandwich was catalytically grown on bifunctional lamellar substrates. The roots of the aligned CNTs were acholared on the graphene sheets, which guaranteed excellent loading transfer between graphene and CNTs at very high stress loading. The as-obtained aligned CNT/graphene sandwich blocks offered an ultrahigh energy absorption density of 237.1 kJ kg^{-1} at 95% strain, and 76.1% of the energy was recovered when the stress was released. 80% energy density was maintained when the compression rate varied from 0.5 to 5 mm min^{-1}, indicating that the aligned CNT/graphene sandwiches afforded a rapid dynamics response and superior rate performance for mechanical energy storage. Furthermore, a reversible energy storage density of 130 kJ kg^{-1}, an energy storage efficiency of 83%, and a power density as high as 10.4 kW kg^{-1} were achieved under cyclic compression of the aligned CNT/graphene sandwiches. The effective connection between CNTs and graphene as well as the aligned packing of CNTs and graphene guarantee the efficient and effective stress transfer along the *c*-axis of CNTs and conjugate graphene planes, and thus render the resilient CNT/graphene frameworks with superior mechanical energy storage performance. Such sandwich offers rational arrangement of graphene and CNTs into anticipated nanostructures with 3D inconnected electron pathways, abundant mesopores, as well as robust scaffolds, which is a novel material platform to demonstrate the instrinsic propertis of nanocarbon hybrids. It is highly expected the sandwich materials may have potential applications in the area of nanocomposite, energy storage, environmental protection, electronic device, as well as healthcare.

4. Experimental

4.1. Catalyst preparation

The vermiculite with a size of 2–5 mm served as the carrier of catalyst was mined in Lingshou, PR China. After exfoliated by heating at 900 °C for 10 min, the exfoliated vermiculite (EV, 20.0 g) was impregnated into an aqueous solution (100 mL) of $Fe(NO_3)_3 \cdot 9H_2O$ (>99.0%, 5.0 g) and $(NH_4)_6Mo_7O_{24} \cdot 4H_2O$ (>99.0%, 1.0 g) through strong stirring for 1.0 h at 80 °C. Subsequently, the uniform suspension was dried at 110 °C for 12.0 h. After washing and filtration, the filtrated cake was further dried at 110 °C for 12.0 h, and then the FeMo/EV catalyst for aligned CNT/graphene sandwich growth was available.

4.2. Aligned CNT/graphene sandwich synthesis and purification

The synthesis of aligned CNT/graphene sandwiches were operated in a quartz tube with an inner diameter of 25 mm and a length of 1200 mm. The as-obtained catalyst was placed uniformly in a quartz boat and introduced into the center of the quartz tube. Typically, the reactor was heated to 650 °C in an atmosphere of Ar (150 sccm) and H_2 (120 sccm). Then C_2H_4 (120 sccm) was introduced into the quartz tube for 15 min to grow aligned CNTs between EV flakes. After that, the quartz reactor was further heated to 950 °C in Ar atmosphere (150 sccm), and then graphene was deposited on the EV flakes at 950 °C for 30 min under an atmosphere of Ar (150 sccm) and CH_4 (120 sccm). After cooling down under Ar flow, the as-obtained products were treated with a HCl (6.0 M) aqueous solution at 80 °C for 12.0 h and a HF (6.0 M) aqueous solution at 80 °C for 12.0 h, subsequently, to remove the catalysts. The aligned CNT/graphene sandwiches were collected for further characterization.

4.3. Characterizations

The morphology of the samples was characterized by a JSM 7401F (JEOL Ltd., Tokyo, Japan) SEM operated at 3.0 kV and a JEM 2010 (JEOL Ltd., Tokyo, Japan) TEM operated at 120.0 kV. The purity of the sandwiches was obtained through thermalgravimetric analysis (TGA) by a TGA/DSC1 STAR^e system under O_2 flow. Raman spectra were recorded with He–Ne laser excitation at 633 nm using a Horiba Jobin Yvon LabRAM HR800 Raman spectrometer. The mechanical energy storage performance was evaluated by an electronic universal testing machine (WDW 3020) equipped with a 20 kN load cell and two steel compression platforms. Typically, a cylindrical die with an inner diameter of 4 mm was placed on the fixed bottom stage, and a block of aligned CNT/graphene sandwiches (*ca.* Φ 4 × 5 mm, with a density of *ca.* 50 mg cm^{-3}) was loaded into the cavity of the die. The top stage was moved down to contact and push the punch downward relative to the die, so that the sample inside was compressed. The compressive stress-strain curves were used to calculate the energy absorption and release density. The compression rates were varied from 0.5 to 5 mm min^{-1} for the characterization of the power performance.

Acknowledgements

We thank helpful discussion with Hong-Jie Peng, Hao-Fan Wang. This work was supported by National Basic Research Program of China (973 Program, 2011CB932602) and Natural Scientific Foundation of China (No. 21306102).

Appendix A. Supporting information

Supplementary data associated with this article can be found in the online version at http://dx.doi.org/10.1016/j.nanoen.2014.05.005.

References

[1] C. Liu, F. Li, L.P. Ma, H.M. Cheng, Adv. Mater. 22 (2010) E28.
[2] R. Sebastian, R.P. Alzola, Renewable Sustainable Energy Rev 16 (2012) 6803.
[3] Z.L. Wang, J.H. Song, Science 312 (2006) 242.
[4] A. Yu, P. Jiang, Z.L. Wang, Nano Energy 1 (2012) 418.
[5] F.-R. Fan, Z.-Q. Tian, Z.L. Wang, Nano Energy 1 (2012) 328.
[6] J. Liang, L. Huang, N. Li, Y. Huang, Y. Wu, S. Fang, J. Oh, M. Kozlov, Y. Ma, F. Li, R. Baughman, Y. Chen, ACS Nano 6 (2012) 4508.

[7] S.Z. Li, X.D. Ding, J. Li, X.B. Ren, J. Sun, E. Ma, Nano Lett. 10 (2010) 1774.
[8] M.F. Yu, O. Lourie, M.J. Dyer, K. Moloni, T.F. Kelly, R.S. Ruoff, Science 287 (2000) 637.
[9] C. Lee, X.D. Wei, J.W. Kysar, J. Hone, Science 321 (2008) 385.
[10] A. Cao, P.L. Dickrell, W.G. Sawyer, M.N. Ghasemi-Nejhad, P.M. Ajayan, Science 310 (2005) 1307.
[11] S.A. Chesnokov, V.A. Nalimova, A.G. Rinzler, R.E. Smalley, J.E. Fischer, Phys. Rev. Lett. 82 (1999) 343.
[12] F.A. Hill, T.F. Havel, C. Livermore, Nanotechnology 20 (2009) 255704.
[13] Z.G. Fthenakis, Z. Zhu, D. Teich, G. Seifert, D. Tomanek, Phys. Rev. B: Condens. Matter 88 (2013) 245402.
[14] R. Zhang, Q. Wen, W. Qian, D.S. Su, Q. Zhang, F. Wei, Adv. Mater. 23 (2011) 3387.
[15] X. Gui, J. Wei, K. Wang, A. Cao, H. Zhu, Y. Jia, Q. Shu, D. Wu, Adv. Mater. 22 (2010) 617.
[16] Z.P. Zeng, X.C. Gui, Z.Q. Lin, L.H. Zhang, Y. Jia, A.Y. Cao, Y. Zhu, R. Xiang, T.Z. Wu, Z.K. Tang, Adv. Mater. 25 (2013) 1185.
[17] Z. Zeng, X. Gui, Q. Gan, Z. Lin, Y. Zhu, W. Zhang, R. Xiang, A. Cao, Z. Tang, Nanoscale 6 (2014) 1748.
[18] X. Gui, Z. Zeng, Y. Zhu, H. Li, Z. Lin, Q. Gan, R. Xiang, A. Cao, Z. Tang, Adv. Mater. 26 (2014) 1248.
[19] M.-Q. Zhao, Q. Zhang, J.-Q. Huang, F. Wei, Adv. Funct. Mater. 22 (2012) 675.
[20] A.L.M. Reddy, S.R. Gowda, M.M. Shaijumon, P.M. Ajayan, Adv. Mater. 24 (2012) 5045.
[21] H.-J. Peng, J.-Q. Huang, M.-Q. Zhao, Q. Zhang, X.-B. Cheng, X.-Y. Liu, W.-Z. Qian, F. Wei, Adv. Funct. Mater. 24 (2014) 2772.
[22] X.C. Gui, A.Y. Cao, J.Q. Wei, H.B. Li, Y. Jia, Z. Li, L.L. Fan, K. L. Wang, H.W. Zhu, D.H. Wu, ACS Nano 4 (2010) 2320.
[23] L. Huang, N. Yi, Y. Wu, Y. Zhang, Q. Zhang, Y. Huang, Y. Ma, Y. Chen, Adv. Mater. 25 (2013) 2224.
[24] H. Hu, Z.B. Zhao, W.B. Wan, Y. Gogotsi, J.S. Qiu, Adv. Mater. 25 (2013) 2219.
[25] Q. Zhang, M. Zhao, Y. Liu, A. Cao, W. Qian, Y. Lu, F. Wei, Adv. Mater. 21 (2009) 2876.
[26] Y. Liu, W.Z. Qian, Q. Zhang, A.Y. Cao, Z.F. Li, W.P. Zhou, Y. Ma, F. Wei, Nano Lett. 8 (2008) 1323.
[27] Z. Fan, J. Yan, L. Zhi, Q. Zhang, T. Wei, J. Feng, M. Zhang, W. Qian, F. Wei, Adv. Mater. 22 (2010) 3723.
[28] S. Li, Y. Luo, W. Lv, W. Yu, S. Wu, P. Hou, Q. Yang, Q. Meng, C. Liu, H.-M. Cheng, Adv. Energy Mater 1 (2011) 486.
[29] L.L. Zhang, Z.G. Xiong, X.S. Zhao, ACS Nano 4 (2010) 7030.
[30] D.H. Lee, J.E. Kim, T.H. Han, J.W. Hwang, S. Jeon, S.-Y. Choi, S.H. Hong, W.J. Lee, R.S. Ruoff, S.O. Kim, Adv. Mater. 22 (2010) 1247.
[31] Y. Zhu, L. Li, C.G. Zhang, G. Casillas, Z.Z. Sun, Z. Yan, G.D. Ruan, Z.W. Peng, A.R.O. Raji, C. Kittrell, R.H. Hauge, J.M. Tour, Nat. Commun 3 (2012) 1225.
[32] M.Q. Zhao, X.F. Liu, Q. Zhang, G.L. Tian, J.Q. Huang, W.C. Zhu, F. Wei, ACS Nano 6 (2012) 10759.
[33] G.K. Dimitrakakis, E. Tylianakis, G.E. Froudakis, Nano Lett. 8 (2008) 3166.
[34] T.-K. Hong, D.W. Lee, H.J. Choi, H.S. Shin, B.-S. Kim, ACS Nano 4 (2010) 3861.
[35] J.J. Shao, W. Lv, Q.G. Guo, C. Zhang, Q. Xu, Q.H. Yang, F.Y. Kang, Chem. Commun. 48 (2012) 3706.
[36] V.C. Tung, L.-M. Chen, M.J. Allen, J.K. Wassei, K. Nelson, R.B. Kaner, Y. Yang, Nano Lett. 9 (2009) 1949.
[37] D. Cai, M. Song, C. Xu, Adv. Mater. 20 (2008) 1706.
[38] F. Du, D. Yu, L. Dai, S. Ganguli, V. Varshney, A.K. Roy, Chem. Mater. 23 (2011) 4810.
[39] Y. Wu, T. Zhang, F. Zhang, Y. Wang, Y. Ma, Y. Huang, Y. Liu, Y. Chen, Nano Energy 1 (2012) 820.
[40] B. Raton, in: M. Madou (Ed.), Fundamentals of Microfabrication, CRC Press, 2002.
[41] A. Sadezky, H. Muckenhuber, H. Grothe, R. Niessner, U. Poschl, Carbon 43 (2005) 1731.
[42] L. Xu, N. Wei, Y. Zheng, Z. Fan, H.Q. Wang, J.C. Zheng, J. Mater. Chem. 22 (2012) 1435.
[43] J. Sun, H. Liu, X. Chen, D.G. Evans, W. Yang, X. Duan, Adv. Mater. 25 (2013) 1125.
[44] N. Jha, P. Ramesh, E. Bekyarova, M.E. Itkis, R.C. Haddon, Adv. Energy Mater 2 (2012) 438.
[45] Z. Yan, L.L. Ma, Y. Zhu, I. Lahiri, M.G. Hahm, Z. Liu, S.B. Yang, C.S. Xiang, W. Lu, Z.W. Peng, Z.Z. Sun, C. Kittrell, J. Lou, W.B. Choi, P.M. Ajayan, J.M. Tour, ACS Nano 7 (2013) 58.
[46] K. Kumar, Y.S. Kim, X. Li, J.J. Ding, F.T. Fisher, E.H. Yang, Chem. Mater. 25 (2013) 3874.
[47] Z.-J. Fan, J. Yan, T. Wei, G.-Q. Ning, L.-J. Zhi, J.-C. Liu, D.-X. Cao, G.-L. Wang, F. Wei, ACS Nano 5 (2011) 2787.
[48] M.Q. Zhao, Q. Zhang, J.Q. Huang, G.L. Tian, T.C. Chen, W.Z. Qian, F. Wei, Carbon 54 (2013) 403.
[49] W. Wang, S. Guo, M. Penchev, I. Ruiz, K.N. Bozhilov, D. Yan, M. Ozkan, C.S. Ozkan, Nano Energy 2 (2013) 294.
[50] W. Wang, I. Ruiz, S. Guo, Z. Favors, H.H. Bay, M. Ozkan, C.S. Ozkan, Nano Energy 3 (2014) 113.
[51] S. Nemat-Nasser, W.J. Kang, J.D. McGee, W.G. Guo, J. B. Isaacs, Int. J. Impact Eng. 34 (2007) 1119.
[52] J. Suhr, P. Victor, L.C.S. Sreekala, X. Zhang, O. Nalamasu, P.M. Ajayan, Nat. Nanotechnol 2 (2007) 417.
[53] T.A. Schaedler, A.J. Jacobsen, A. Torrents, A.E. Sorensen, J. Lian, J.R. Greer, L. Valdevit, W.B. Carter, Science 334 (2011) 962.

Cheng Tang graduated from the department of chemical engineering, Tsinghua University, PR China, in 2013, and is currently a Ph.D. candidate there. His research interests are interfacial chemistry, synthesis chemistry, hierarchical nanocarbon, nanocomposite materials, and their applications in catalysis and energy conversion and storage.

Qiang Zhang graduated in 2004 from the department of chemical engineering, Tsinghua University, China, where he continued doing research on mass production of carbon nanotubes and obtained his Ph.D. in chemical engineering in 2009. After a short stay as a research associate in Case Western Reserve University, USA in 2009, he joined the Fritz Haber Institute of the Max Planck Society, Germany as a post-doctoral fellow. He was appointed an associate professor of chemical engineering of Tsinghua University in 2011. His current research interests are nanocarbon, hierarchical nanostructures, energy conversion and storage.

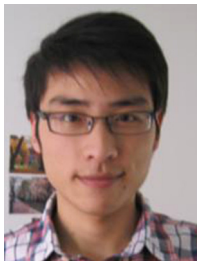

Meng-Qiang Zhao obtained his Ph.D. in chemical engineering from Tsinghua University (PR China) in 2013. He is currently a post-doctoral researcher in the A.J. Drexel Nanomaterials Institute in Drexel University, USA. His research interests are the synthesis and property studies of carbon nanomaterials for electrochemical energy storage.

Gui-Li Tian obtained her B.S. degree in 2010 in department of chemical engineering and technology, Tianjin University and then joined Tsinghua University where she is currently pursuing her Ph.D. in chemical engineering. Her research involves the synthesis of nitrogen doped nanocarbons including carbon nanotubes and graphene and their application in energy storage and conversion systems.

Fei Wei obtained his Ph.D. in chemical engineering from China University of Petroleum in 1990. After a postdoctoral fellowship at Tsinghua University, he was appointed an associate professor in 1992 and professor of chemical engineering of Tsinghua University in 1996. He was also a Visiting Professor at Ohio State University (USA), University of Western Ontario (Canada), and Nagoya Institute of Science and Technology (Japan). Now he is the director of the Fluidization Laboratory of Tsinghua University. His scientific interests are chemical reaction engineering, multiphase flow, advanced materials, and sustainable energy.